Journal of the Korean Magnetic Resonance Society **2015**, *19*, 29-35
DOI 10.6564/JKMRS.2015.19.1.029

Ferroelectric-Paraelectric Phase Transition of CsH_2PO_4 studied by Static NMR and MAS NMR

Ae Ran Lim[1*] and Kwang-Sei Lee[2]

[1]Department of Science Education, Jeonju University, Jeonju 560-759, Korea
[2]Department of Nano Science & Engineering, Center for Nano Manufacturing, Inje University, Gimhae 621-749, Korea

Received Mar 31, 2015; Revised May 4, 2015; Accepted May 14, 2015

Abstract The microscopic dynamics of CsH_2PO_4, with two distinct hydrogen bond lengths, are studied by static nuclear magnetic resonance (NMR) and magic angle spinning (MAS) NMR. The proton dynamics of the two crystallographically inequivalent hydrogen sites were discussed in terms of the ^1H NMR and ^1H MAS NMR spectra. Although the hydrogen bonds have two inequivalent sites, H(1) and H(2), distinct proton dynamics for the two sites were not found. Further, the ^{133}Cs spectrum is more or less continuous near T_{C1} (=153 K). Finally, the phase transition mechanism of T_{C1} in CsH_2PO_4 is related to the ordering of protons.

Keywords Single crystal; Structural geometry; Ferroelectric; Nuclear magnetic resonance

Introduction

Anhydrous proton-conducting materials have attracted interest in recent years because of their potential applications in fuel cells[1]. Cesium dihydrogen phosphate, CsH_2PO_4, belongs to a group of compounds that have properties intermediate between those of a normal salt and an acid, and undergoes a transition from a paraelectric phase to a superprotonic phase at 503 K (=T_{C2})[2–6]. It is well known that the superionic phase transition of CsH_2PO_4 from the monoclinic to the cubic phase significantly increases its protonic conductivity[7, 8]. Recent advances in solid acid fuel cells have demonstrated the usefulness of pure CsH_2PO_4 as an electrolyte in both hydrogen and direct methanol fuel cells[9]. The proton transport mechanism in solid acids is a subject of intensive experimental and theoretical studies[10-12]. However, the simultaneous decomposition and dehydration of CsH_2PO_4 above 500 K complicate the interpretation of the phenomena[13–16]. CsH_2PO_4 belongs to a family of structurally disordered protonic conductors that possess superionic phases[17]. It exhibits one of the largest conductance values in the high temperature phase. In addition, the CsH_2PO_4 crystal undergoes a phase transition at 153 K (=T_{C1}) and exhibits ferroelectricity below 153 K. It has a second-order ferroelectric phase transition with spontaneous polarization along the monoclinic *b* axis[18–20].
Yamada et al. [21] investigated the paraelectric to superionic phase transition of CsH_2PO_4 by using X-ray diffraction and nuclear magnetic resonance (NMR). They suggested a reorientational jump of the

* Address correspondence to: **Ae Ran Lim**, Tel: +82-(0)63-220-2514; Fax: +82-(0)63-220-2053; E-mail: aeranlim@hanmail.net, arlim@jj.ac.kr

$H_2PO_4^-$ anion above 420 K from the temperature dependence of the ^1H and ^{31}P NMR results. Further, Iwata et al. [22] found that the phase transition of T_{C1} in CsH_2PO_4 was also connected with a rotation of the PO_4 tetrahedra. The ionic conduction behavior of the superprotonic phase of CsH_2PO_4 was recently examined by determining the ^1H NMR spin–lattice relaxation time[23]. In addition, the temperature variation in the electric field gradient (EFG) tensor at the ^{133}Cs sites in CsH_2PO_4 has been reported in the paraelectric and ferroelectric phases. The EFG tensor components decrease in absolute value with decreasing temperature, showing no anomaly at T_{C1} [24]. Further, the ^{133}Cs spin–lattice relaxation time of CsH_2PO_4 has been determined near T_{C1}, and the anomalously short values of T_1 were found to be a result of the critical temperature dependence[25]. Previously, Blinc et al.[25] investigated this relaxation rate over the phase transition temperature range, albeit at a much lower field. Furthermore, the theory that describes the temperature dependence of ^{133}Cs T_1 was developed on the basis of proton dynamics and of how it affects EFG fluctuations on the ^{133}Cs sites. This result shows how the spin-lattice relaxation rate of ^{133}Cs peaks at T_{C1}, showing critical behavior, and drops back to a steady and larger value, only a few kelvin away from the transition temperature.

In this study, we examine the integrated signal area, NMR spectrum, and spin–lattice relaxation times in the laboratory frame, T_1, and in the rotating frame, $T_{1\rho}$, for ^1H and ^{133}Cs in CsH_2PO_4 in the ferroelectric and paraelectric phases, respectively. The well separated static NMR and magic angle spinning (MAS) NMR line components of the crystallographically inequivalent proton sites in CsH_2PO_4 have provided us with a unique opportunity to study the distinct proton dynamics associated with the different hydrogen bond lengths. In this work, we are able to distinguish between the sites of the two inequivalent protons in CsH_2PO_4, H(1) and H(2).

Crystal Structure

The CsH_2PO_4 crystal undergoes two phase transitions, at T_{C1}=153 K and T_{C2}=503 K. At room temperature, the CsH_2PO_4 paraelectric phase has a monoclinic structure with space group C_{2h}^2 ($P2_1/m$), and the lattice constants are a=7.912 Å, b=6.383 Å, c=4.882 Å, β=107.73°, and Z=2 [26–28]. The crystal structure in the paraelectric phase is depicted in Fig. 1[29]. Below T_{C2}=503 K, the paraelectric phase of CsH_2PO_4 possesses a monoclinic structure with two crystallographically different hydrogen bonds between PO_4 units, forming a one-dimensional hydrogen bond network[30-32]. The hydrogen bonds along the b-axis, H(2), form a zigzag chain consisting of short hydrogen bonds (2.48 Å), and those along the c-axis, H(1), form a linear chain consisting of slightly longer hydrogen bonds (2.54 Å). Cs atoms and PO_4 groups are centered on mirror planes perpendicular to the b-axis. Above 503 K, the cubic structure has a lattice constant of a=4.9615 Å, and the space group is $Pm3m$. Below T_{C1}, the crystal structure of ferroelectric CsH_2PO_4 is monoclinic with space group C_2^2 ($P2_1$), and the lattice constants are a=7.904 Å, b=6.316 Å, c=4.895 Å, β= 108.23º, and Z =2[33].

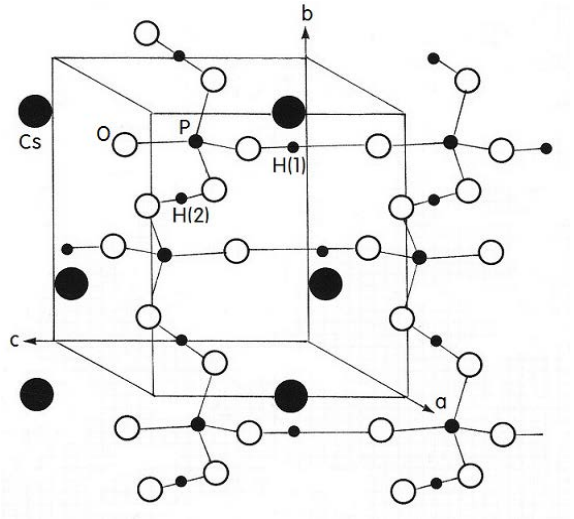

Figure 1. Crystal structure of CsH_2PO_4 in paraelectric phase.

Experimental Method

CsH_2PO_4 single crystals were grown by slow evaporation from an aqueous solution at room temperature, following the reaction: $Cs_2CO_3 + 2H_3PO_4 \rightarrow 2CsH_2PO_4 + CO_2\uparrow + H_2O$[34]. The crystals were parallelepipedic and colorless. The

crystallographic *c*-axis was determined from the crystal morphology.

The NMR signals and the spin–lattice relaxation time in the laboratory frame, T_1, for ^1H nuclei in CsH_2PO_4 single crystals were measured using the Varian 200 MHz NMR and 500 MHz NMR spectrometers at the Korea Basic Science Institute Seoul Western Center. The static magnetic fields were 4.7 T and 11.75 T, respectively, and the central radio frequencies were set to $\omega_o/2\pi$=200 MHz and $\omega_o/2\pi$=500 MHz for the ^1H nucleus. The spectrum and relaxation times were obtained with the magnetic field applied parallel to the *c*-axis of the crystal. We measured the ^1H T_1 using a saturation recovery pulse sequence *sat*–*t*–π/2. The nuclear magnetizations of the ^1H nuclei at a time *t* after the *sat* pulse (a comb of one hundred π/2 pulses applied at a regular interval of 2 μs) and the delay time of 420 μs were determined following the excitation π/2 pulse. Also, sixteen scans were employed for the acquisition of spectra. The widths of the π/2 pulses were 3 μs for ^1H at 200 MHz and 1 μs for ^1H at 500 MHz. Further, the NMR signals and spin–lattice relaxation times in the laboratory frame, T_1, for ^{133}Cs nuclei in CsH_2PO_4 single crystals were measured using the Varian 200 MHz NMR, Bruker 400 MHz NMR, and Varian 500 MHz NMR spectrometers at the Korea Basic Science Institute Seoul Western Center. The central radio frequencies were set to $\omega_o/2\pi$=26.23 MHz, 52.48 MHz, and 65.57 MHz, respectively, for the ^{133}Cs nucleus. The ^{133}Cs T_1 measurements were performed using *sat*–*t*–π/2 pulse sequences. The nuclear magnetization M(*t*) of the ^{133}Cs nuclei at a time *t* after the *sat* pulses was determined from the saturation recovery sequence following each pulse. The width of the π/2 pulse was 4 μs for ^{133}Cs.

The ^1H MAS NMR experiments were performed at a Larmor frequency of 400 MHz. The samples were placed in the 4 mm MAS probe as powders, and the MAS rate was set to 10 kHz for ^1H MAS to minimize the spinning sideband overlap. The spin–lattice relaxation times in the rotating frame, $T_{1\rho}$, for ^1H were measured by applying a spin-locking pulse. The π pulse time for ^1H was 5 μs according to the spin-locking field. The NMR measurements were obtained in the temperature range of 100–425 K. The sample temperatures were maintained at constant values by controlling the helium gas flow and heater current, yielding an accuracy of ±0.5 K.

Results and Discussion

The NMR spectrum of ^1H (I=1/2) in CsH_2PO_4 crystals was obtained at frequencies of 200 MHz above 200 K and 500 MHz below 200 K. Here, the experiments were performed upon cooling below 300 K and upon heating above 300 K. The H resonance lines of the CsH_2PO_4 crystal were obtained with the magnetic field applied along the crystallographic *c*-axis. The NMR spectrum of ^1H in the CsH_2PO_4 crystal as a function of temperature below 200 K is shown in two dimensions in Fig. 2. The resonance line of the lower resonance frequency can be attributed to the H(1) hydrogen site of the longer hydrogen bond, and that of the higher resonance frequency can be attributed to the H(2) hydrogen site of the shorter hydrogen bond. This assignment of ^1H NMR lines was supported by the result of the spin-lattice relaxation time $T_{1\rho}$ in the rotating frame.

The two ^1H resonance lines for H(1) and H(2) overlap, and the intensity of the lines for H(2) is stronger than that of those for H(1). Fig. 3 shows the integration of the two ^1H NMR signals shown in Fig. 2; the integrated signals were measured at $\omega_o/2\pi$=500 MHz.

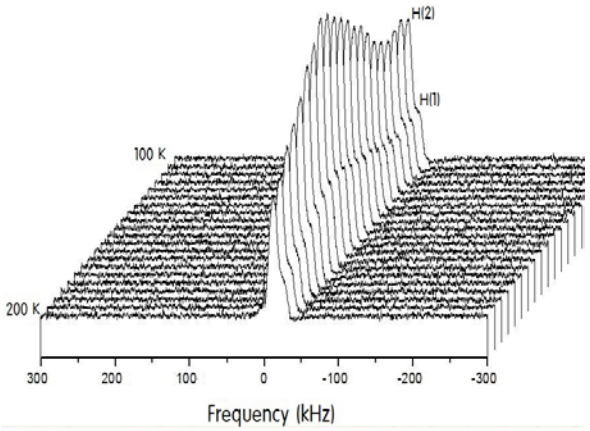

Figure 2. ^1H NMR spectrum of CsH_2PO_4 single crystal as a function of temperature ($\omega_o/2\pi$=500 MHz).

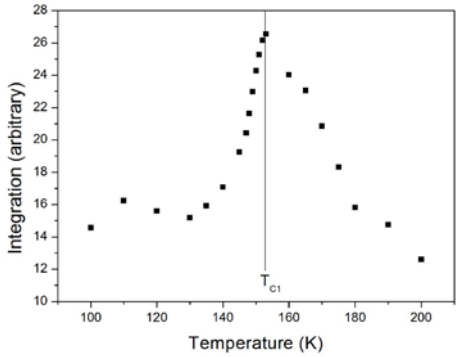

Figure 3. Integrated ^{1}H NMR spectrum of CsH_2PO_4 single crystal as a function of temperature

The integration increases with increasing temperature below T_{C1}, and near T_{C1} the integration is strong. Above T_{C1}, the integration decreases abruptly with increasing temperature. Prompted by the published result that dynamic ordering of hydrogen occurs in one of the hydrogen bonds as the material enters the ferroelectric phase, we propose that the change in the proton-signal intensity with temperature is related to the ordering of these protons[35].

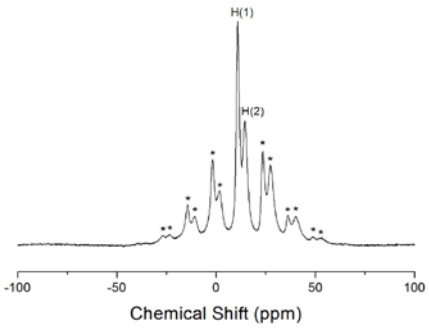

Figure 4. ^{1}H MAS NMR spectrum of CsH_2PO_4 at room temperature ($\omega_o/2\pi$=400 MHz).

MAS NMR was used for detailed analysis of the structure of the two protons in CsH_2PO_4. Fig. 4 shows the ^{1}H MAS NMR spectrum of CsH_2PO_4 at room temperature. The NMR spectrum consists of two peaks, at chemical shifts of δ=10.95 ppm and δ=14.58 ppm. The spinning sidebands are marked with asterisks. The line component with the smaller chemical shift can be attributed to the H(1) hydrogen site of the longer hydrogen bond, and that with the greater chemical shift can be attributed to the H(2) hydrogen site of the shorter hydrogen bond.

The nuclear magnetization recovery curves of the ^{1}H nuclei were obtained by measuring the nuclear magnetization at several temperatures. The temperature dependence of the spin–lattice relaxation time in the laboratory frame, T_1, by static NMR and in the rotating frame, $T_{1\rho}$, by MAS NMR for ^{1}H in CsH_2PO_4 was obtained, as shown in Fig. 5. The ^{1}H relaxation times of the CsH_2PO_4 crystal at the two Larmor frequencies of 200 and 500 MHz show strong frequency dependence compared to the two T_1 data at 300 K at both frequencies. The spin–lattice relaxation time T_1 for the H nuclei measured at 500 MHz decreases with increasing temperature, and the T_1 values are very long. T_1 is continuous near T_{C1}.

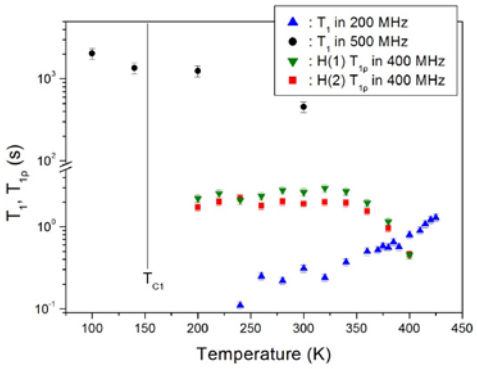

Figure 5. Temperature dependence of spin-lattice relaxation time in the laboratory frame, T_1, and in the rotating , $T_{1\rho}$, for ^{1}H in CsH_2PO_4.

Further, the spin–lattice relaxation time T_1 for the H nuclei measured 200 MHz in the paraelectric phase increases with increasing temperature, and the T_1 values are short. Here, the opposite trends for T_1 with increasing temperature are measured. This means that the molecular motions produced by T_1 can be vary according to the strength of the magnetic field. The NMR results for the T_1 values may depend strongly on the magnetic field. The 200 MHz and 400 MHz NMR spectroscopy measurements did not have adequate temperature control at low temperature, whereas those at 500 MHz did. The relaxation time obtained by 500 MHz NMR spectroscopy could not be measured at several temperatures because of the long proton relaxation time. In addition, the $T_{1\rho}$

values in the paraelectric phase were obtained at $\omega_o/2\pi$ = 400 MHz, as shown in Fig. 5. Here, the $T_{1\rho}$ values for H(1) are longer than those for H(2). This result is consistent with the length of the hydrogen bond. Smaller values of T_1 and $T_{1\rho}$ indicate an easier transfer of energy from the nuclear spin system to the surroundings. From the crystal structure, the H(2) protons, which form short hydrogen bonds, are expected to display shorter relaxation times than the H(1), which form slightly longer hydrogen bonds. Therefore, the H(1) and H(2) spectra are assigned using the T_1 and $T_{1\rho}$ values obtained here. Near 400 K, the $T_{1\rho}$ values decrease abruptly with increasing temperature.

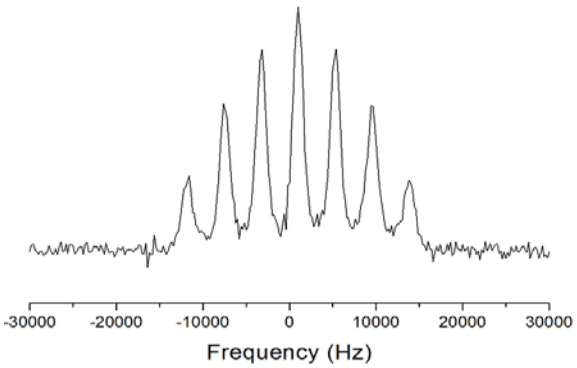

Figure 6(a). ^{133}Cs NMR spectrum of CsH_2PO_4 single crystal at 145 K ($\omega_o/2\pi$=65.57 MHz).

The resonance lines of ^{133}Cs (I=7/2) in CsH_2PO_4 crystals were observed at frequencies of 26.23 MHz, 52.48 MHz, and 65.57 MHz when the magnetic field was applied along the *c*-axis of the crystal. The ^{133}Cs NMR spectrum at a frequency of 65.57 MHz at 145 K is shown in Fig. 6(a). The satellite transitions are well resolved from the central line, and the signal

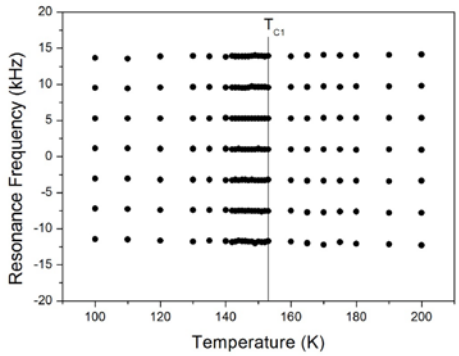

Figure 6(b). ^{133}Cs NMR spectrum of CsH_2PO_4 single crystal as a function of temperature ($\omega_o/2\pi$=65.57 MHz).

intensity of the central line is stronger than those of the other lines. The splitting of the ^{133}Cs resonance lines was not change over a wide temperature range, as shown in Fig. 6(b). The zero point of the *y*- axis shows the resonance frequency, 65.57 MHz, of the ^{133}Cs nucleus. The central transition is virtually unshifted by the quadrupole interaction, and the relationships between the lines vary slightly with temperature. Further, the splitting between the resonance lines near T_{C1} is continuous, showing no anomaly. This result is consistent with that of Kanda and Fujimura[24]. Because of the low quadrupole coupling constants of the ^{133}Cs nuclei, the central transition is not shifted by the quadrupole interaction.

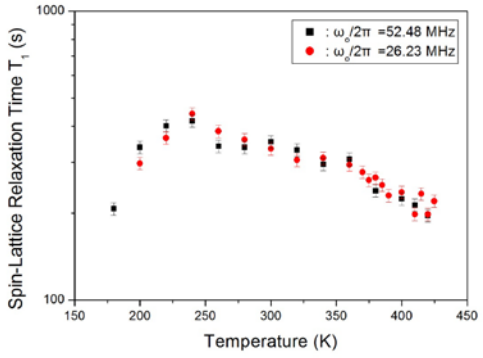

Figure 7. Temperature dependence of spin-lattice relaxation time in the laboratory frame, T_1, for ^{133}Cs in CsH_2PO_4 single crystal.

The spin–lattice relaxation times of ^{133}Cs in a CsH_2PO_4 single crystal were measured at two frequencies, 26.23 MHz and 52.48 MHz. The recovery traces of the magnetizations for this crystal were measured at several different temperatures. We measured the variations with temperature of the relaxation times for the central resonance line for the ^{133}Cs nuclei at these two frequencies. The recovery traces for the central resonance line of ^{133}Cs in the CsH_2PO_4 crystal can be represented by a single exponential function. The saturation recovery traces vary with the delay time. The ^{133}Cs relaxation times were then determined directly from the slopes of the log $[M(\infty) - M(t)]/M(\infty)$ versus time (t) plots[35-38]. The temperature dependence of the ^{133}Cs spin–lattice relaxation time T_1 in the CsH_2PO_4 crystals is shown in Fig. 7. The ^{133}Cs relaxation times for a CsH_2PO_4 crystal at the two Larmor frequencies of 26.23 and

52.48 MHz are frequency independent. Above 240 K, the ^{133}Cs T_1 value decreases slowly with increasing temperature, and the T_1 of ^{133}Cs above 240 K undergoes slow motion. The spin–lattice relaxation time for ^{133}Cs is very long in this temperature range investigated here.

Conclusion

We studied the microscopic dynamics of CsH_2PO_4, with two distinct hydrogen bond lengths, by static NMR and MAS NMR. The distinct proton dynamics of the two crystallographically inequivalent hydrogen sites were discussed in terms of the ^{1}H NMR and ^{1}H MAS NMR spectra. The crystal structure of LiH_2PO_4 was recently examined using single-crystal neutron diffraction, which elucidated two types of hydrogen bonds with different bond lengths[34]. The CsH_2PO_4 crystal structure has two different hydrogen bond lengths as well as the structure of LiH_2PO_4. Although the hydrogen bonds have crystallographically inequivalent sites, H(1) and H(2), distinct proton dynamics for the two sites were not found. Further, the change in the integrated proton signal near T_{C1} in CsH_2PO_4 is related to the ordering of protons.

The microscopic dynamics of ^{1}H and ^{133}Cs in CsH_2PO_4 in the ferroelectric and paraelectric phases were also studied by examining the spin–lattice relaxation times in the laboratory frame, T_1, and in the rotating frame, $T_{1\rho}$. The ^{1}H $T_{1\rho}$ value decreases abruptly with increasing temperature, and the decrease can be ascribed to the onset of slow translational diffusion of protons[39,40]. The ^{133}Cs spectrum is more or less continuous near T_{C1}. The ^{1}H relaxation times at three Larmor frequencies show a strong frequency dependence, whereas the ^{133}Cs relaxation times at two Larmor frequencies are frequency independent. Consequently, the phase transition near T_{C1} in CsH_2PO_4 is due to the ordering of protons, whereas it is not due to the Cs ions.

Acknowledgements

This research was supported by the Basic Science Research program through the National Research Foundation of Korea (NRF) funded by the Ministry of Education, Science and Technology (2015021274).

References

1. H. S. Lee and M. E. Tuckerman, *J. Phys. Chem*. C **112**, 9917 (2008)
2. J. Otomo, T. Ishigooka, T. Kitano, H. Takahashi, and H. Nagamoto, *Electrochimica Acta* **53**, 8186 (2008)
3. J. Otomo, N. Minagawa, C. Wen, K. Eguchi, and H. Takahashi, *Solid State Ionics* **156**, 356 (2003)
4. D. A. Boysen, S. M. Haile, H. Liu, and R. A. Secco, *Chem. Mater*. **15**, 727 (2003)
5. W. Bronowska, *J. Chem. Phys*. **114**, 611 (2001)
6. A. I. Baranov, V. P. Khiznichenko, V. A. Sandler, and L. A. Shuvalov, *Ferroelectrics* **81**, 1147 (1988)
7. A. I. Baranov, E. M. Kopnin, V. V. Grebenev, A. Sin, Yu. Dubitsky, and P. Caracino, *Phys. Stat. Solidi* A **206**, 36 (2009)
8. S. M. Haile, C. R. I. Chisholm, K. Sasaki, D. A. Boyser, and T. Uda, *Faraday Discuss* **134**, 17 (2007)
9. S. Hossein, W. R. W. Daud, M. Badiei, A. A. H. Kadhum, and A. B. Mohammad, *Bull. Mater. Sci*. **34**, 759 (2011)
10. B. V. Merinov and U. Bismayer, *Solid State Ionics* **136**, 223 (2000)
11. R. E. Lechner, *Solid State Ionics* **145**, 167 (2001)
12. B. Merinov, *Solid State Ionics* **213**, 72 (2012)
13. E. Ortiz, R. A. Vargas, and B.-E. Mellander, *J. Chem. Phys*. **110**, 4847 (1999)
14. Y. K. Taninouchi, T. Uda, Y. Awakura, A. Ikeda, and S. M. Haile, *J. Mater. Chem*. **17**, 3182 (2007)

15. A. I. Baranov, E. M. Kopnin, V. V. Grebenev, A. Zaopo, Yu. Dubitsky, and P. Caracino, *Solid State Ionics* **178**, 657 (2007)
16. Y.-K. Taninouchi, T. Uda, and Y. Awakura, *Solid State Ionics* **178**, 1648 (2008)
17. V. G. Ponomareva and E. S. Shutova, *Russian J. Electrochem*. **43**, 513 (2007)
18. E. Kanda, A. Tamaki, and T. Fujimura, *J. Phys*. C **15**, 3401 (1982)
19. R. Youngblood, B. C. Frazer, J. Eckert, and G. Shirane, *Phys. Rev*. B **22**, 228 (1980)
20. M. Wada, A. Sawada, and Y. Ishibashi, *J. Phys. Soc. Jpn*. **47**, 1571 (1979)
21. K. Yamada, T. Sagara, Y. Yamane, and H. O. Okuda, *Solid State Ionics* **175**, 557 (2004)
22. Y. Iwata, N. Koyano, and I. Shibuya, *J. Phys. Soc. Jpn*. **49**, 304 (1980)
23. A. Ishikawa, H. Maekawa, T. Yamamura, Y. Kawakita, K. Shibata, and M. Kawai, *Solid State Ionics* **179**, 2345 (2008)
24. E. Kanda and T. Fujimura, *J. Phys. Soc. Jpn*. **43**, 1813 (1977)
25. R. Blinc, B. Lozar, B. Topic, and S. Zumer, *J. Phys. C: Solid State Phys*. **16**, 5053 (1983)
26. H. Matsunaga, K. Itoh, and E. Nakamura, *J. Phys. Soc. Jpn*. **48**, 2011 (1980)
27. C. E. Botez, J. D. Hermosillo, J. Zhang, J. Qian, Y. Zhao, J. Majzlan, R. R. Chianelli, and C. Pantea, *J. Chem. Phys*. **127**, 194701 (2007)
28. J. Hatori, Y. Matsuo, and S. Ikehata, *Solid State Ionics* **178**, 681 (2007)
29. Y. Shchur, *Phys. Rev*. B **74**, 54301 (2006)
30. E. J. Sonneveld and J. W. Wisser, *Acta Crystallogr*. **35**, 1975 (1979)
31. D. Semmingsen, W. D. Ellenson, B. S. Frazer, and G. Shirane, *Phys. Rev. Lett*. **38**, 1299 (1971)
32. Y. Uesu and J. Kobayashi, *Phys. Stat. Solidi* A **34**, 475 (1976)
33. L.N. Rashkovich, K.B. Meteva, *Sov. Phys. Crystallogr*. **23**, 447 (1978)
34. I. H. Oh, K.-S. Lee, M. Meven, G. Heger, and C. E. Lee, *J. Phys. Soc. Jpn*. **79**, 74606 (2010)
35. O. V. Rozanov, Yu. N.Moskvich, and A. A. Sukhovskii, *Sov. Phys. Solid State* **25**, 212 (1983)
36. A. Abragam, "The Principles of Nuclear Magnetism" Chap. 3, Oxford University Press, Oxford, 1961.
37. I. G. Lee, K.-Y. Lee, J.-H. Kim, S. Chae, and H.-J. Lee, *J. Kor. Mag. Reson*. **17**, 54 (2013)
38. Y. K. Paik and C. L. Chang, *J. Kor. Mag. Reson*. **17**, 19 (2013)
39. R. K. Harris, "Nuclear Magnetic Resonance Spectroscopy" Chap. 5, Pitman Pub. INC, London, 1983.
40. A. Damyanovich, M. M. Pintar, and R. Blinc, J. Slak, *Phys. Rev*. B **56**, 7942 (1997)